
This is an electronic reprint of the original article.
This reprint may differ from the original in pagination and typographic detail.

Yosri, A.; Leheta, H.; Saad-Eldeen, S.; Zayed, A.

Accumulated fatigue damage assessment of side structural details in a double hull tanker based on spectral fatigue analysis approach

Published in:
Ocean Engineering

DOI:
[10.1016/j.oceaneng.2022.111069](https://doi.org/10.1016/j.oceaneng.2022.111069)

Published: 01/05/2022

Document Version
Publisher's PDF, also known as Version of record

Published under the following license:
CC BY

Please cite the original version:
Yosri, A., Leheta, H., Saad-Eldeen, S., & Zayed, A. (2022). Accumulated fatigue damage assessment of side structural details in a double hull tanker based on spectral fatigue analysis approach. *Ocean Engineering*, 251, Article 111069. <https://doi.org/10.1016/j.oceaneng.2022.111069>

This material is protected by copyright and other intellectual property rights, and duplication or sale of all or part of any of the repository collections is not permitted, except that material may be duplicated by you for your research use or educational purposes in electronic or print form. You must obtain permission for any other use. Electronic or print copies may not be offered, whether for sale or otherwise to anyone who is not an authorised user.



Accumulated fatigue damage assessment of side structural details in a double hull tanker based on spectral fatigue analysis approach

A. Yosri^{a,b,*}, H. Leheta^b, S. Saad-Eldeen^c, A. Zayed^b

^a School of Engineering, Department of Mechanical Engineering, Aalto University, Espoo, Finland

^b Faculty of Engineering, Department of Naval Architecture & Marine Engineering, Alexandria University, Egypt

^c Faculty of Engineering, Department of Naval Architecture & Marine Engineering, Port Said University, Egypt

ARTICLE INFO

Keywords:

Fatigue damage
Spectral fatigue analysis
Spectral method
Corrosion
Corrosion fatigue

ABSTRACT

The fatigue life of structural details in the double side of a tanker ship was investigated, employing the spectral fatigue analysis approach. The stochastic environmental loads were derived by seakeeping software based on the 3D diffraction theory, in the frequency domain, and then mapped on a structural finite element model for the ship hull. The stress response at the considered details was extracted from the finite element analysis and the accumulated damage was estimated by Palmgren-Miner's rule. The reduction of the hull girder section modulus and the deterioration of fatigue strength due to corrosion were taken into account. The influences of different wave scatter diagrams, reduction of hull girder section modulus, stress concentration factor, free corrosion S-N curve, wave direction, wave spectrum and operational profile on the accumulated fatigue damage were investigated.

1. Introduction

Ocean-going ships operate in a corrosive environment and are subjected to complex cyclic loads. These loads are mainly excited by waves and different operational profiles. The interaction between the corrosive environment and these cyclic loads provokes corrosion fatigue cracks. These cracks extensively deteriorate the fatigue strength comparing with the effect of corrosion as a thickness reduction only. The most susceptible locations to fatigue cracks are the welded joints where high-stress concentration, residual stress, misalignments and welding imperfections are expected. Therefore, a lot of the studies that investigate the fatigue damage of marine structures usually focus on the accumulated damage of the welded joints at various critical locations.

In the recent decades, many methods have been introduced and improved with the gained experience to estimate the fatigue life of marine structures. The selection of a suitable method is essential for a reliable fatigue damage assessment. These methods may be categorized under two main approaches; the damage tolerance approach and the safe life approach. The former is based on fracture mechanics theories and assumes the existence of fatigue cracks, while the latter estimates the crack initiation and propagation life based on an appropriate category of the S-N curves. The S-N curve approaches are usually employed

in the beginning of the design stage. However, various uncertainties in the estimated fatigue life are expected. Those uncertainties arise primarily from the adopted S-N curve and the estimated cyclic fatigue loads (Lotsberg, 2019). Many S-N curves are suggested by the design standards based on the load type and the considered structural detail. These standards are not always precise or sufficient to select an adequate fatigue strength curve, especially, in a free corrosion environment (Aeran et al., 2017). The accurate determination of the cyclic fatigue loads is a time-consuming process containing a lot of uncertain statistics. Recently, the use of powerful software with improved knowledge from the past experience has reduced the uncertainty in the stress response analysis; which in turn reduced the uncertainty in the estimated fatigue life of marine structures.

Within the past few years, there has been a growing commitment to introduce more precise fatigue assessment methodologies based on the safe life approach (Yue et al., 2021; Du et al., 2015). Although these methods may have potential improvement in the fatigue damage estimation; the simplified method, deterministic fatigue analysis, spectral fatigue analysis and time-domain fatigue analysis are thus far commonly adopted in the marine field (Bai and Jin, 2015; American Bureau of Shipping, 2003). The selection of the appropriate method depends on the available data and the required accuracy. The simplified method assumes Weibull distribution for the stress range; thus, the resulting

* Corresponding author. School of Engineering, Department of Mechanical Engineering, Aalto University, Espoo, Finland.

E-mail addresses: Yosri.hassan@aalto.fi, ahmed.yosri@alexu.edu.eg (A. Yosri), heba.leheta@alexu.edu.eg (H. Leheta), saad.bahey@eng.psu.edu.eg (S. Saad-Eldeen), Ahmedzayd@hotmail.com (A. Zayed).

<https://doi.org/10.1016/j.oceaneng.2022.111069>

Received 19 November 2021; Received in revised form 23 January 2022; Accepted 7 March 2022

Available online 25 March 2022

0029-8018/© 2022 The Author(s). Published by Elsevier Ltd. This is an open access article under the CC BY license (<http://creativecommons.org/licenses/by/4.0/>).

Nomenclature	
K_g	Geometric Stress Concentration Factor SCF
ω	Wave frequency
ω_e	Encounter wave frequency
ω_p	Spectral peak frequency
T_p	Peak wave period
T_z	Zero up-crossing period
H_s	Significant wave height
L_w	Wavelength
L_{pp}	Length between perpendicular
γ_j	JONSWAP spectral shape parameter
$\sigma, \sigma_a, \sigma_b$	Spectral width parameters
σ_t	Tensile stress
σ_c	Compressive stress
σ_r	Stress range
σ_i	Root mean square of the stress response spectrum
x	$\sigma_r^2/8\sigma_i^2$
$\Delta\sigma_n$	Nominal stress range
θ	Ship heading direction
U	Ship forward speed
$H_\sigma(\omega_e \theta)$	Stress transfer function
$S_\sigma(\omega_e H_s, T_z, \theta)$	Stress response spectrum
$S_\eta(\omega_e H_s, T_z)$	Wave spectrum
$S_{PM}(\omega)$	Two-parameter Pierson–Moskowitz (PM) spectrum
$S_j(\omega)$	JONSWAP (Joint North Sea Wave Project) wave spectrum
S_e	Stress range at the Bi-linear S–N curve knee point
$f_S(\theta')$	Spreading function
f_m	Mean stress correction factor
i	Sea state index
j	Wave heading direction index
μ_n	n th spectral moment of stress response
T_{02i}	Average stress cycle period of sea state
T_{life}	Duration of stationary response process
ν_{0i}	zero-up crossing frequency
$F_i(\sigma_r)$	Rayleigh distribution function of stress range response
$p(\sigma_r)$	Rayleigh probability density function of stress range response
$N(\sigma_r)$	Number of cycles to failure corresponding to a stress range σ_r
$n(\sigma_r)$	Number of stress range (σ_r) cycles
m_1, K_1	Slope and scale parameter of a single slope S–N curve or a Bi-linear S–N curve when $N \leq 10^7$ cycles
m_2, K_2	Slope and scale parameter of a Bi-linear S–N curve when $N > 10^7$ cycles
D_{fat}	Accumulated damage
Γ	Complementary incomplete gamma function
γ	Incomplete Gamma function
z	Gamma function integral limits
$R_m(t)$	Section modulus reduction as a function of time t
NA	North Atlantic wave scatter diagram
WW	Worldwide wave scatter diagram
P-M	Pierson–Moskowitz spectrum
FL	Fully loaded condition
SFA	Spectral Fatigue Analysis

fatigue damage is extensively sensitive to the presumed Weibull shape parameter. Also, the deterministic method is not accurate enough due to the complex and stochastic nature of the marine environment (Du et al., 2015; American Bureau of Shipping, 2003). The spectral fatigue method has become more reliable for offshore and floating marine structures by the virtue of its reasonable estimation of the stress response and the fatigue damage (Thompson, 2016; Magoga, 2020). On the other hand, it is a time-consuming approach and computationally intensive. It is noteworthy that each method may result in a considerably different estimation of fatigue damage for the same structure detail, as reported by Wang (2010) and Rörup et al. (2017). In addition, it is difficult to judge which method is more appropriate for a specific framework.

The spectral fatigue analysis approach accounts more precisely for the dynamic effects and waves irregularity. Hence, it requires more comprehensive descriptions of the environmental data, loading conditions and operational profiles (Bai and Jin, 2015; Rörup et al., 2017). The method simulates the time history of the structural response by a linear superposition. The hydrodynamic loads and their corresponding stress response spectrum of each short-term sea state are first estimated. The accumulated fatigue damage is then calculated employing Palmgren–Miner’s rule, whereas, the linear addition of all the encountered sea states damages gives the long-term value. Theoretically, once it reaches unity, the fatigue failure will occur. Failure here does not necessarily imply a complete collapse of the structural detail but maybe the beginning of losing its ability to withstand loads.

1.1. Uncertainties in fatigue analysis

Different literatures addressed the sources of uncertainties in the numerical fatigue damage assessment (Garbatov and Guedes Soares, 2012; Wirsching and Chen, 1988; Shetty, 1997; Guedes Soares et al., 2003). These uncertainties originate from the mean stress of the applied load, stress concentration, weld imperfections and residual stresses, S–N

curves and in addition to the scatter diagrams. The contribution of cargo inertial forces to the accumulated fatigue damage may be added to the above uncertainties. However, it can be conservatively neglected at specific locations on the ship side (Xue et al., 1994). Palmgren–Miner’s rule assumes that failure occurs once the linear summation of fatigue damages of all sea states equals 1. Despite significant efforts were done to investigate its shortcomings and to propose alternative methods (Santecchia et al., 2016), Palmgren–Miner’s rule is still widely applied in the marine field owing to its intrinsic simplicity.

To simplify the computational intensity of the fatigue numerical analysis, many literatures only considered the wave-induced vertical bending moment (Kukkanen and Mikkola, 2004; Nguyen et al., 2013) as the only important cyclic loading that induces stresses on deck structural details. Others included the effect of wave-induced horizontal bending moments as introduced by Wang (2010). The remaining load types as the lateral and torsional loads are usually ignored. The implementation of the seakeeping and finite element software in spectral fatigue analysis was presented in different literatures (Guedes Soares et al., 2003; Li et al., 2013). Coupling the latest development in seakeeping and finite element can omit the uncertainties in the loads and the structural response. However, the other statistical uncertainties still exist.

Although, the spectral fatigue assessment shows good consistency with full-scale measurements (Thompson, 2016; Magoga, 2020) and is widely adopted in classification societies rules (DNV CN, 2014; ABS, 2017), its reliance on the frequency domain is occasionally questionable. This is because the frequency domain analysis, considering linear potential flow theory or strip theory, does not take into account the non-linear ship response due to hull girder loads and local stresses at the intermittent wet and dry surfaces within splash zones. The non-vertical hull form at the bow and stern induces asymmetry sagging and hogging responses which are prominent in fine ships and in case of encountering high wave amplitudes. Guedes Soares et al. (Guedes Soares and Schellin, 1998) studied the nonlinear wave-induced bending moment of three

tankers. It has been shown that the bending moment is linear in large tankers while it depicts significant non-linearity in small ones. Nevertheless, the fatigue damage is dominated by moderate wave amplitudes (Nguyen et al., 2013; Li et al., 2013), and therefore, in practice, the non-linearity in hull girder loads and material performance can be ignored. The local pressure applied on intermittent wet and dry surfaces mainly affects the side structural details near and below the splash zone, particularly, at the intersections between side longitudinal and transverse bulkheads (Fricke and Wittenberg, 1995; Fricke et al., 1995). This dynamic pressure can be evaluated separately and then incorporated in the frequency domain analysis with the hull girder loads (DNV CN, 2014; Folsø, 1998) or it can be precisely estimated by carrying out non-linear analysis. Zhiyuan Li et al. (2013) studied the impact of non-linearity on the fatigue damage of a side structural detail, located below the mean waterline, in a Panamax containership. No remarkable difference in the linear and nonlinear fatigue results is stated for the considered detail and methodology, which indicates that the relatively simple spectral fatigue analysis is still precise in many locations of the ship side.

The deterioration of the material fatigue and tensile strengths due to corrosion is well documented in the literature based on experiments (Garbatov et al., 2014a, 2014b, 2019) and numerical analysis (Yosri et al., 2020, 2021; Nguyen et al., 2012). The synergistic interactions between cyclic loads, material microstructure and corrosive environment over time spur the corrosion-fatigue cracking (Li and Akid, 2013). Despite the revival of the corrosion-fatigue studies, several long-term fatigue analyses research were conducted on the premise that the corrosion fatigue does not occur and hence, they only used the S–N curve in air. This may be because in the early design stage there is no consensus on the optimal time to apply the corrosion fatigue S–N curve due to the complex quantitative modelling of this phenomenon. Nevertheless, for coated ballast tanks, DNV (DNV CN, 2014) suggested applying corrosion S–N curve after the end of the effective corrosion protection period, which is taken to be the last five years of the ship's design life. While for other locations rather than the ballast tanks, e.g., external hull, cargo oil tanks, ... etc., the S–N curve in air can be used for the specified design life. Tran Nguyen et al. (2013) compared the evaluated fatigue damage of a tanker deck structural detail using an S–N curve in air (thickness deterioration was considered) and in corrosive environment. They applied the corrosion S–N curve at the age of 6.5 years, which yielded a significant reduction of the fatigue life compared with the one evaluated by the S–N curve in air. Therefore, corrosion fatigue is one of the critical uncertainties involved in the fatigue analysis. It reflects the importance of the regular maintenance of coating in ballast tanks throughout the ship's operational life time.

1.2. The objective of the current study

The present study combines the latest developments of seakeeping and finite element analyses (FEA) together in the fatigue analysis employing the spectral approach. Most of the research in this area employs the classical beam theory together with the conventional strip theory and usually considers only the vertical bending moment, which cannot guarantee accurate fatigue damage estimation. The main advantage of using the seakeeping and FEA softwares is obtaining precise stress response considering a more accurate presentation of the hydrodynamics loads, complex structural details and their interactions. The accurate estimation of fatigue damage cannot be attained without taking into account the corrosion degradation as an ageing factor. Therefore, using the 3D diffraction theory, the present study investigates the accumulated fatigue damage of two side structural details above and below the water level of a crude oil tanker considering corrosion degradation. Several conclusions have been addressed indicating the main sources of uncertainties in the accumulated fatigue damage that the designer should consider in the detailed design stage.

2. Spectral fatigue analysis

2.1. Case study

The case study adopted here is an unrestricted service crude oil tanker. Its main particulars and mid-ship section properties are given in Fig. 1. The tanker has high tensile steel (AH32) deck and sheer strake, while the remaining parts are constructed from Grade (A) mild steel with modulus of elasticity 200 GPa and Poisson ratio 0.3. The studied connections are located within the side structure portion built from Grade (A) steel as indicated in Fig. 1. The structural configuration as well as plan and 3D model of the considered details are presented in Fig. 2. The considered details are substantially loaded by the hull girder loads, while the second detail is subject to additional external still water and wave induced loads. It has to be stressed that the details are located in corrosive environment, where the double side is used as ballast tanks with variable water levels according to the desired immersion. According to DNVGL (DNVGL CG, 2015), the first fatigue crack is expected to initiate at the hotspot point "a" (Fig. 2) on the weld toe before propagating through the thickness of the side longitudinal flange or stiffener web. The geometric stress concentration factor K_g of detail 1 at Point "a" when the longitudinal is subject to axial load equals 1.28 according to DNVGL Class guideline (DNVGL CG, 2015). To exclude the effect of stress concentration factor when comparing the fatigue life of both details, it is assumed that detail 2 has the same geometric stress concentration as detail 1. For the considered worldwide trading tanker, the fraction of time at sea, in loaded or ballast conditions, is taken as 42.5% of a target operational life of 25 years as recommended by DNV (DNV CN, 2014).

2.2. Description of the irregular seas

The irregularity of the ocean surface can be simplified by a superposition of large number of regular waves of different frequencies, directions and heights. Based on this simplification, the wave can be described mathematically for the spectral fatigue analysis. The wave energy within each sea state (assumed stationary for 1.86 hour) is a relatively narrow-banded Gaussian random process, which can be demonstrated by the wave spectrum. There is a large set of standardized wave spectra available in the design standards. The most commonly used wave spectra are the two-parameter Pierson–Moskowitz (PM) spectrum (DNVGL, 2018) and JONSWAP (Joint North Sea Wave Project) wave spectrum (Hasselmann et al., 1973) which has a sharper peak and applies to the growing waves in continental-shelf waters.

The P–M and JONSWAP spectrum are given as

$$S_{PM}(\omega) = \frac{5}{16} \cdot H_s^2 \cdot \omega_p^4 \cdot \omega^{-5} \cdot \exp\left(-\frac{5}{4} \left(\frac{\omega}{\omega_p}\right)^{-4}\right) \quad (1)$$

$$S_J(\omega) = [1 - 0.287 \cdot \ln(\gamma_J)] \cdot S_{PM}(\omega) \cdot \gamma_J^{\exp\left(-0.5 \left(\frac{\omega - \omega_p}{\sigma \omega_p}\right)^2\right)} \quad (2)$$

where ω is the wave frequency in *rad/sec*, ω_p is the spectral peak frequency = $2\pi/T_p$, T_p is the spectral peak period, H_s is the significant wave height, σ is the spectral width parameter; $\sigma = \sigma_a$ for $\omega \leq \omega_p$, $\sigma = \sigma_b$ for $\omega > \omega_p$ and γ_J is a non-dimensional peak shape parameter.

The correlation between the zero up-crossing period T_z and the wave peak period T_p is given as follows:

$$\frac{T_z}{T_p} = 0.6673 + 0.05037 \gamma_J - 0.00623 \gamma_J^2 + 0.0003341 \gamma_J^3 \quad (3)$$

The wave data collected during the JONSWAP experiment shows that average values for γ_J , σ_a and σ_b are 3.3, 0.07 and 0.09, respectively.

Two formulations for the JONSWAP spectrum were employed. One has a single peak with a shape parameter $\gamma_J = 3.3$ and in the second

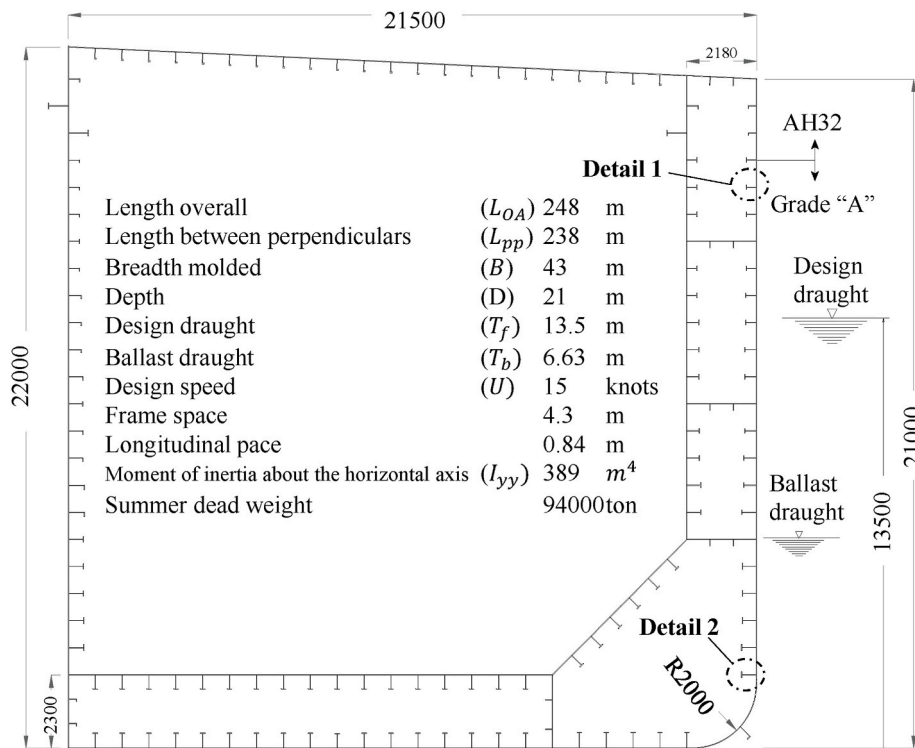


Fig. 1. Midship section of the oil tanker and its principal dimensions.

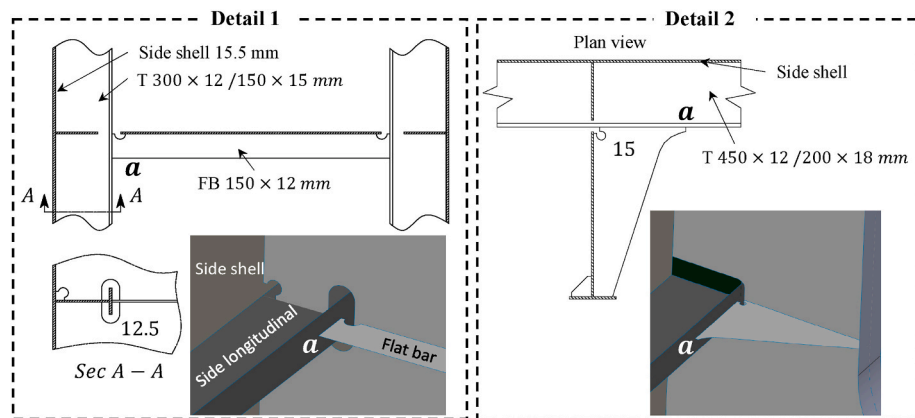


Fig. 2. Plan and 3D view of the considered details.

formulation, γ_J was calculated from equation (4) as recommended by DNVGL (2018).

$$\begin{aligned} \gamma_J &= 5 && \text{for } T_p / \sqrt{H_s} \leq 3.6 \\ \gamma_J &= \exp\left(5.75 - 1.15 \frac{T_p}{\sqrt{H_s}}\right) && \text{for } 3.6 < T_p / \sqrt{H_s} < 5 \\ \gamma_J &= 1 && \text{for } 5 \leq T_p / \sqrt{H_s} \end{aligned} \quad (4)$$

The long-term probability of occurrence of the different sea states within specific regions is given in the wave scatter diagrams. The North Atlantic scatter diagram is usually adopted in fatigue life design for vessels that sail frequently in the North Atlantic and/or in other harsh environments (DNV CN, 2014). Another general practice is adopting the worldwide scatter diagram which covers many nautical zones, including North Pacific and North Atlantic.

2.3. Stress response spectrum

The objective of the stress response analysis is to define the stress response spectra of each sea state and operating condition. Thereafter, these spectra are the main inputs for the spectral fatigue analysis. Despite, the substantial computational effort needed to conduct this analysis using FE method compared with that needed using beam theory, FE method gives considerable accurate results, particularly, if combined with the direct application of the hydrodynamic loads. The assumption of the linear ship response to the wave excitation can facilitate the calculation of the stress response and, in consequence, the fatigue analysis using spectral method (Guedes Soares and Schellin, 1998; Guedes Soares, 1993), without remarkable reduction in the accuracy. Based on the linear assumption, the stress transfer function $H_\sigma(\omega_e|\theta)$ can reveal the stress response at the structural detail per unit wave amplitude as a function of the encounter wave frequency ω_e and heading direction θ . It should be defined for each loading condition and

forward speed (U). The calibration of the stress transfer functions is described in the following sections. Each stress transfer function is then used to calculate the stress response spectrum, $S_{\sigma}(\omega_e|H_s, T_z, \theta)$, by scaling the wave energy spectrum in the following manner:

$$S_{\sigma}(\omega_e|H_s, T_z, \theta) = |H_{\sigma}(\omega_e|\theta)|^2 S_{\eta}(\omega_e|H_s, T_z) \quad (5)$$

where H_s is the significant wave height of the sea state and $S_{\eta}(\omega_e|H_s, T_z)$ is the wave spectrum experienced by the ship which represents the wave energy (or wave amplitude) distribution of each individual encounter wave frequency in a stationary sea state (frequency domain).

The n^{th} spectral moment of the stress response can be described as:

$$\mu_n = \int_0^{\infty} \omega_e^n \cdot S_{\sigma}(\omega_e|H_s, T_z, \theta) d\omega_e \quad (6)$$

For a given sea state (i), a spreading function $f_s(\theta')$ maybe introduced to the spectral moment to include the wave spreading (Guedes Soares, 1995) of confused short-crested sea conditions as given by Eq. (7).

$$\mu_{ni} = \int_0^{\infty} \sum_{\theta=\frac{\pi}{2}}^{\theta+\frac{\pi}{2}} f_s(\theta') \cdot \omega_e^n \cdot S_{\sigma}(\omega_e|H_s, T_z, \theta) d\omega_e \quad (7)$$

where the spreading function is modelled using the cosine-squared approach:

$$f_s(\theta') = \begin{cases} \frac{2}{\pi} \cos^2(\theta'), & \theta - \frac{\pi}{2} \leq \theta' \leq \theta + \frac{\pi}{2} \\ 0, & \text{otherwise} \end{cases} \quad (8)$$

The average stress cycle period is:

$$T_{02i} = \frac{1}{\nu_{0i}} = 2\pi \sqrt{\frac{\mu_{0i}}{\mu_{2i}}} \quad (9)$$

where ν_{0i} is the zero-up crossing frequency. For a narrow-banded response process, the stress range response σ_r in each stationary sea state (i) is Rayleigh distributed:

$$F_i(\sigma_r) = 1 - \exp\left(-\frac{\sigma_r^2}{8\mu_{0i}}\right) \quad (10)$$

The Rayleigh probability density function for the stress range:

$$p(\sigma_r) = \frac{\sigma_r}{4\sigma_i^2} \exp\left(-\frac{\sigma_r^2}{8\sigma_i^2}\right) \quad (11)$$

where σ_i is the root mean square of the response process:

$$\sigma_i = \sqrt{\mu_{0i}} \quad (12)$$

Hence, the long-term stress range distribution can be defined by summing-up the short-term Rayleigh distributions of the stress range within each sea state, accounting for the weightings of the expected sea states from the scatter diagram and the directions and probabilities of the different operational profiles.

2.4. S-N curves

Employing Palmgren-Miner's rule for estimating the accumulated fatigue damage, caused by random time-varying load, requires a well-defined S-N curve which is derived based on experimental data from a constant amplitude fatigue test. The equation of the bi-linear S-N curve has the following form:

$$\begin{aligned} N(\sigma_r) &= K_1 \cdot \sigma_r^{-m_1} \text{ when } N \leq 10^7 \\ N(\sigma_r) &= K_2 \cdot \sigma_r^{-m_2} \text{ when } N > 10^7 \end{aligned} \quad (13)$$

where N is the predicted number of cycles to failure for stress range σ_r (MPa), m is the inverse slope of the S-N curve and K is the scale parameter. The subscript 1 denotes the first slope of the S-N curve, and 2 denotes the second slope.

The fatigue life of the considered details may be divided into two time periods. In the first period, the corrosion protection system is effective, with no corrosion fatigue; thus, the S-N curve in air can be employed. The second period begins once the corrosion protection system breaks down and severe pitting corrosion starts to form (DNVGL CG, 2015). The fatigue life is too sensitive to the free corrosion period and hence; the free corrosion S-N curve should be employed. Once it starts, the accumulated damage will surge up considerably. However, the accumulation of corrosion wastage on the corroded surface may prevent the contact with the corrosive environment and stop the corrosion fatigue (Guedes Soares and Garbatov, 1999). This consideration is beyond the scope of this paper. Nevertheless, it is presumed that the second period commences at the beginning of the hull girder section modulus loss, after 6.5 years of operation as suggested by Guo et al. (2008), and at an age of 20 years as recommended by DNV classification notes (DNV CN, 2014). The results of the two presumptions are investigated in section 4.

The selection of the appropriate welded joint S-N curve from the design standards depends on the joint classification, the existence of corrosion, and the applied stress type (nominal, hotspot or notch stress). The hotspot S-N curve suggested by DNV classification notes (S-N curve I) (DNV CN, 2014) was employed in this study. The curve can be utilized for details fully protected against corrosion. It is defined by the following parameters, $K_1 = 1.45781E + 12$, $K_2 = 4.038E + 15$, $m_1 = 3$ and $m_2 = 5$. Also, employing a single slope S-N curve may be more reliable as reported by Sarkani (Sarkani et al., 1994). The fatigue damage using bilinear and single slope S-N curves has been investigated.

The free corrosion S-N curve (D) suggested by DNVGL recommended practice (DNV GL RP-C203, 2014) was employed in this study. The curve has a single slope with the following parameters; $m_{1c} = 3$ and $K_{1c} = 4.86391E + 11$ (Fig. 3).

The extracted stresses from the coarse mesh FEA in this study yield a global/nominal stress σ_n . The hotspot stress range corresponding to the adopted S-N curves equals $\Delta\sigma_n K_g$.

2.5. Mean stress correction

The residual stresses in welded joints may reach the yield stress magnitude in tension. Therefore, tensile stresses may still act on the welded joints during the compressive stress cycles, which imply fatigue damage as in the case of the tension cycles (Webster and Ezeilo, 2001). Therefore, residual stresses have a negative impact on the fatigue life of welded details. In the numerical fatigue analysis, this negative impact is usually compensated by ignoring the positive effect of the compressive mean stresses. On the other hand, it was shown that welding and construction residual stresses decrease over time as the ship is exposed to external loading and hence, the mean stress correction will be significant and can be applied (Rörup, 2005). If the mean stress effect is considered, the stress range should be multiplied by the mean stress correction factor f_m (DNV CN, 2014). Here, both the tensile and compressive stresses, σ_t and σ_c , respectively, include the stresses induced by the stillwater loads.

$$f_m = \frac{\sigma_t + 0.7 \cdot |\sigma_c|}{\sigma_t + |\sigma_c|} \quad (14)$$

2.6. Fatigue damage

The spectral method assumes a narrow-banded response within each sea state. Hence, the accumulated damage of each sea state, employing Palmgren-Miner's rule, may be expressed in the continuous form:

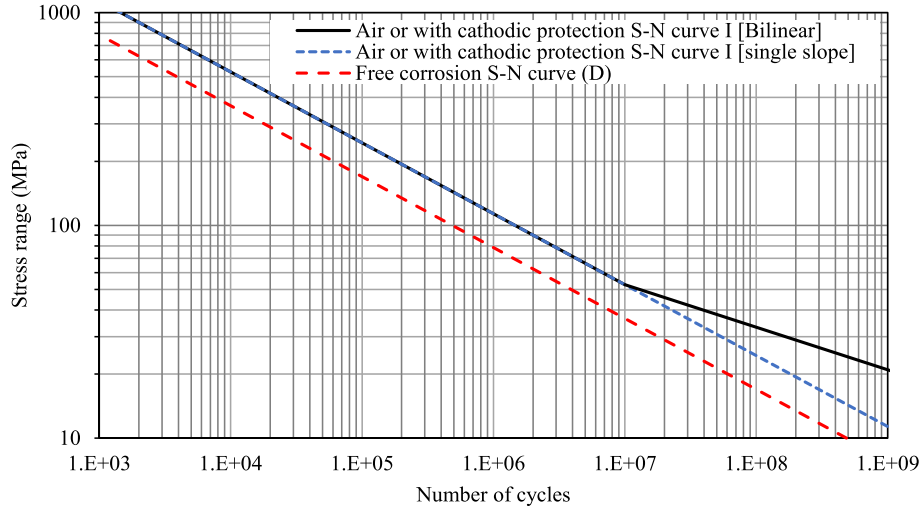


Fig. 3. Adopted S–N curves; air or with cathodic protection S–N curve I [single slope and bilinear] and Free corrosion S–N curve (D).

$$D_{fat} = \int_0^{\infty} \frac{n(\sigma_r)}{N(\sigma_r)} d\sigma_r \quad (15)$$

where $n(\sigma_r)d\sigma_r$ is the number of stress cycles with a stress range between σ_r and $\sigma_r + d\sigma_r$, where σ_r has a Rayleigh distribution. Within a stationary response process of duration T_{life} , $n(\sigma_r)d\sigma_r$ is:

$$n(\sigma_r)d\sigma_r = \frac{T_{life}}{T_{02i}} p(\sigma_r) d\sigma_r = \nu_{0i} T_{life} p(\sigma_r) d\sigma_r \quad (16)$$

Then the fatigue damage using a single slope S–N curve will equal:

$$D_{fat} = \nu_{0i} T_{life} \int_0^{\infty} \frac{p(\sigma_r)}{N(\sigma_r)} d\sigma_r = \frac{\nu_{0i} T_{life}}{K_1} \int \frac{\sigma_r^{m_1+1}}{4\sigma_i^2} \exp\left(-\frac{\sigma_r^2}{8\sigma_i^2}\right) d\sigma_r \quad (17)$$

If $\sigma_r^2 / (8\sigma_i^2) = x$, the gamma function can be expressed as:

$$\Gamma\left(1 + \frac{m_1}{2}\right) = \int_0^{\infty} e^{-x} x^{\frac{m_1}{2}} dx \quad (18)$$

Hence the accumulated fatigue damage of a given loading condition for all sea states (i) and heading directions (j) with joint probability of occurrence p_{ij} can be calculated using the following equation:

$$D_{fat} = \sum_i^{all\ sea-states} \sum_j^{all\ directions} p_{ij} \frac{\nu_{0ij} T_{life}}{K_1} \cdot (8\mu_{0ij})^{\frac{m_1}{2}} \cdot \Gamma\left(1 + \frac{m_1}{2}\right) \quad (19)$$

In case that the adopted S–N curve is bi-linear, the accumulated fatigue damage is (DNV CN, 2014):

$$D_{fat} = \sum_i^{all\ sea-states} \sum_j^{all\ directions} p_{ij} \frac{\nu_{0ij} T_{life}}{K_1} \cdot (8\mu_{0ij})^{\frac{m_1}{2}} \cdot \Gamma\left(1 + \frac{m_1}{2}, z\right) + \sum_i^{all\ sea-states} \sum_j^{all\ directions} p_{ij} \frac{\nu_{0ij} T_{life}}{K_2} \cdot (8\mu_{0ij})^{\frac{m_2}{2}} \cdot \gamma\left(1 + \frac{m_2}{2}, z\right) \quad (20)$$

The complementary incomplete gamma function Γ and the incomplete Gamma function γ are defined as:

$$\Gamma\left(1 + \frac{m_1}{2}, z\right) = \int_z^{\infty} e^{-x} x^{\frac{m_1}{2}} dx \quad (21)$$

$$\gamma\left(1 + \frac{m_2}{2}, z\right) = \int_0^z e^{-x} x^{\frac{m_2}{2}} dx \quad (22)$$

$$\text{and } z = \left(\frac{S_e}{2\sqrt{2}\mu_{0ij}}\right)^2 \quad (23)$$

where S_e is the stress range at the knee point (at 10^7 cycles for S–N curve I).

3. Stress transfer function

3.1. Hydrodynamic model and diffraction analysis

The linear seakeeping analysis was conducted using the commercial software ANSYS Aqwa (ANSYS Aqwa, 2013). The main advantage of using ANSYS Aqwa is the ability to couple the hydrodynamic analysis with the structural FE model. Aqwa simulates the waves' hydrodynamic pressure on the diffracting elements after defining the ship's displacement, center of gravity and inertia about the center of mass. The ship's mass, center of gravity and inertia can be derived from the structural model after defining all main gravitational loads, individually, as point masses. Hence, the accelerations in the hydrodynamic model are derived using one mass element with 6 moments of inertia. Meshing of the hydro model (Fig. 4-a and Table 1) is carried out using Aqwa. The element size dominates the maximum wave frequency that can be utilized in the diffraction analysis. Besides, Aqwa has a limit to the total number of diffracting elements (ANSYS Aqwa, 2013). The adopted mesh size gives a maximum allowable frequency of 0.336 Hz, which is sufficient to cover the realistic frequency range of the transfer functions.

The diffraction analysis, in frequency domain, was conducted by Aqwa for each forward speed and loading condition. In order to define the stress response spectrum for each sea state accurately, the hydrodynamic diffraction analysis should include a wide range of wave frequencies. In this study, the defined wave frequencies are between 0.2 rad/sec to 1.8 rad/sec. Due to the symmetry about the centerline, it is sufficient to consider only the waves coming from one side. Five wave directions were defined between the head sea (-180°) and the beam sea (-90° , waves approach from the portside) with an interval of 22.5° which results in equal probabilities for each direction. Thus, the wave directions between (-90° , portside) to ($+90^\circ$, starboard side) can be defined without affecting the accuracy of the stress response. For instance, if the considered structural detail is located on the starboard side under a stress response of a wave heading with an angle of $+135^\circ$ the stress response of the opposite structural detail at the portside will represent a wave heading with an angle of -135° .

The tanker is designed to travel at a maximum speed of 15 knots

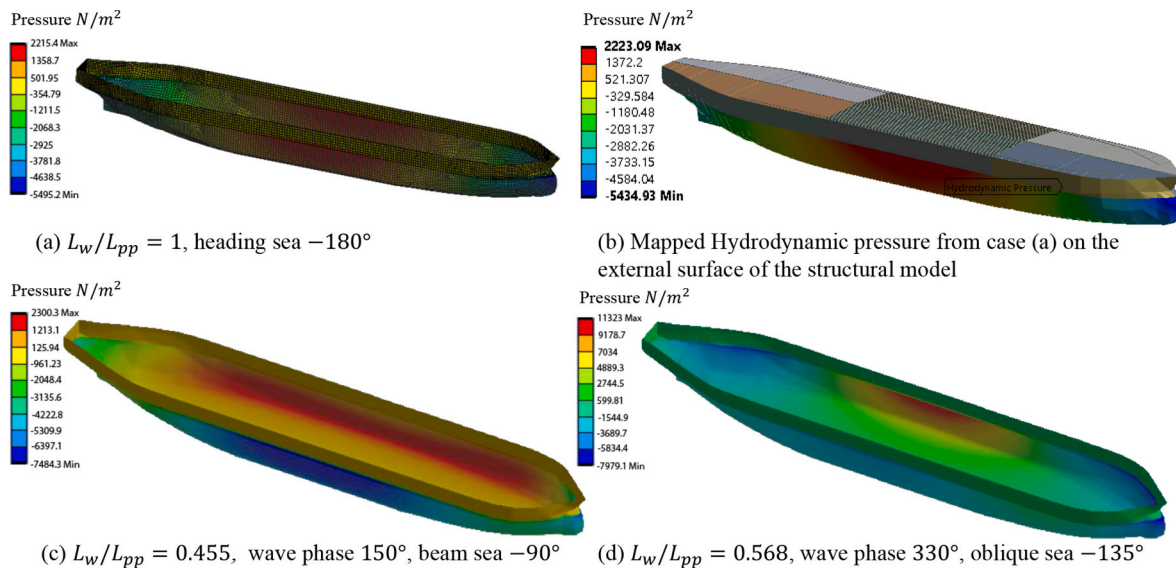


Fig. 4. Hydrodynamic pressure per unit wave height corresponding to the maximum stress response at detail 1 for three different wave headings (fully loaded condition).

Table 1

Mesh information of the hydro model.

Total nodes	7903
Total elements	7734
Diffracting nodes	5186
Diffracting elements	5030

under stationary sea states with significant wave height H_s up to 3.5 m. When $7.5 \text{ m} \geq H_s > 3.5 \text{ m}$, the travel speed is presumed to equal 10 knots; for $11.5 \text{ m} \geq H_s > 7.5 \text{ m}$ the speed will be 5 knots; and zero speed is presumed for higher wave heights.

The analysis was performed 8 times for the different combinations of four forward speeds and two loading conditions; fully loaded and ballast conditions. Therefore, the hydrodynamic analysis can cover all the expected operational profiles and environmental loads. By solving the hydrodynamic diffraction model in frequency domain, the hydrodynamic pressure on each diffracting panel can be calculated. The hydrodynamic pressure includes the incident wave pressure (Froude-Krylov pressure) from the pressure in the undisturbed waves, diffraction pressure due to stationary ship disturbing the incident waves and the radiation pressure due to the diffracting structure's oscillation which generates waves. The linear solution of the Froude-Krylov and the restoring hydrostatic forces are obtained by integrating the pressure up to the predefined waterline of each loading condition. Therefore, the wave pressure above the waterline is always zero and negative pressure exists below it as seen in Fig. 4. This linear assumption may affect the accuracy of the fatigue results in the splash zones, whereas its effect diminishes towards the main deck (Fricke and Wittenberg, 1995; Folso, 1998). If the wave phase represents the relative position of regular wave crest with respect to the center of gravity; Fig. 4 (a, c and d) illustrates the hydrodynamic pressure over the diffracting panels for wave phases and frequencies that result in maximum stress response in head, beam and oblique seas at the considered structural detail 1.

3.2. Structural model

The hydrodynamic pressure generated by Aqwa was mapped on the hull surface of the FE structural model to investigate the stress response induced by a specific regular wave at the considered structural detail as seen in Fig. 4(b). The structural model has the same external hull surface

of the hydro model. Therefore, the interpolation of the hydrodynamic pressure from the centers of the hydrodynamic mesh elements onto the nodes of the structural mesh can be conducted precisely. The dead-weight and lightweight, as crude oil cargo, ballast, engines, superstructure, ...etc., were modelled as point masses within the structural surface boundaries. All structural members were meshed using SHELL181 element, as presented in Fig. 5. A maximum element size of 700 mm is employed which gives stress response with sufficient accuracy in relatively rational computational time. The resulting number of nodes and elements are 212,630 and 283,261, respectively.

To run the structural analysis, the structural model should be free-floating body, without explicit boundary conditions; and the wave pressure should be balanced by the inertial loading. This inertial load is calculated by Aqwa-WAVE (a load transfer and balancing program) based on the hydrodynamic model, mass and inertia. However, the inertial load does not exactly balance the wave pressure due to the small errors in mapping and other differences between structural and hydrodynamic models. Therefore, weak spring is activated in Ansys mechanical to remove the free body singularities. The formation of the transfer functions of each loading condition is illustrated in the flow-chart presented in Fig. 6.

3.3. Stress response

The stress response for each short-term sea state is obtained for several frequencies, from 6 to 10 frequencies, to establish the stress transfer function with an acceptable accuracy. The number and values of those frequencies depend mainly on the shape of the stress response curve, see Fig. 7, and the natural frequency of the ship. Therefore, it is a matter of judgement. It is not practical to calculate numerically the stress response for many frequencies as it is a time-consuming process. However, to maintain the precision of the integration of the corresponding stress response spectrum, spline interpolation was employed to define points of very small intervals between the numerically calculated discrete points. Hence, the full range of the transfer function can be defined smoothly.

The total number of load cases for which the tanker should be analyzed equals the product of the number of the selected wave phases (12 phases with equal interval), wave frequencies, wave directions, forward speeds and loading conditions. The result will be a number of transfer functions equals the product of the number of wave directions, forward speeds and loading conditions. It is noteworthy that, the stress

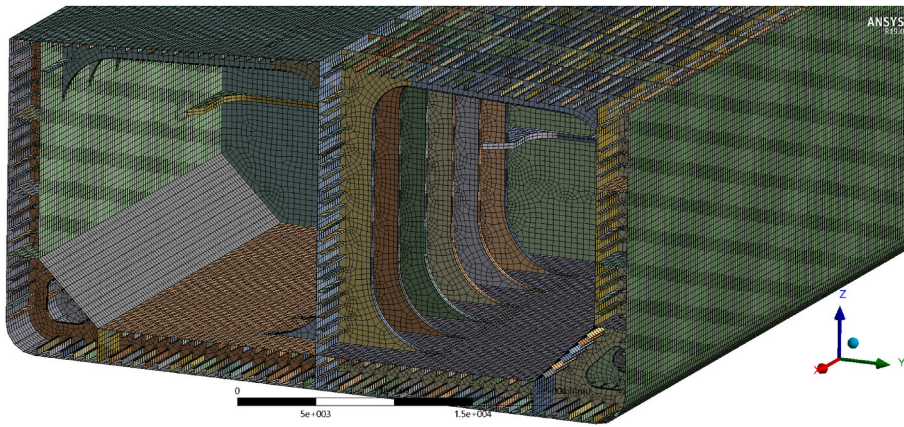


Fig. 5. Structural finite element model for a hull module in the parallel middle body and the typical mesh employed (SHELL181).

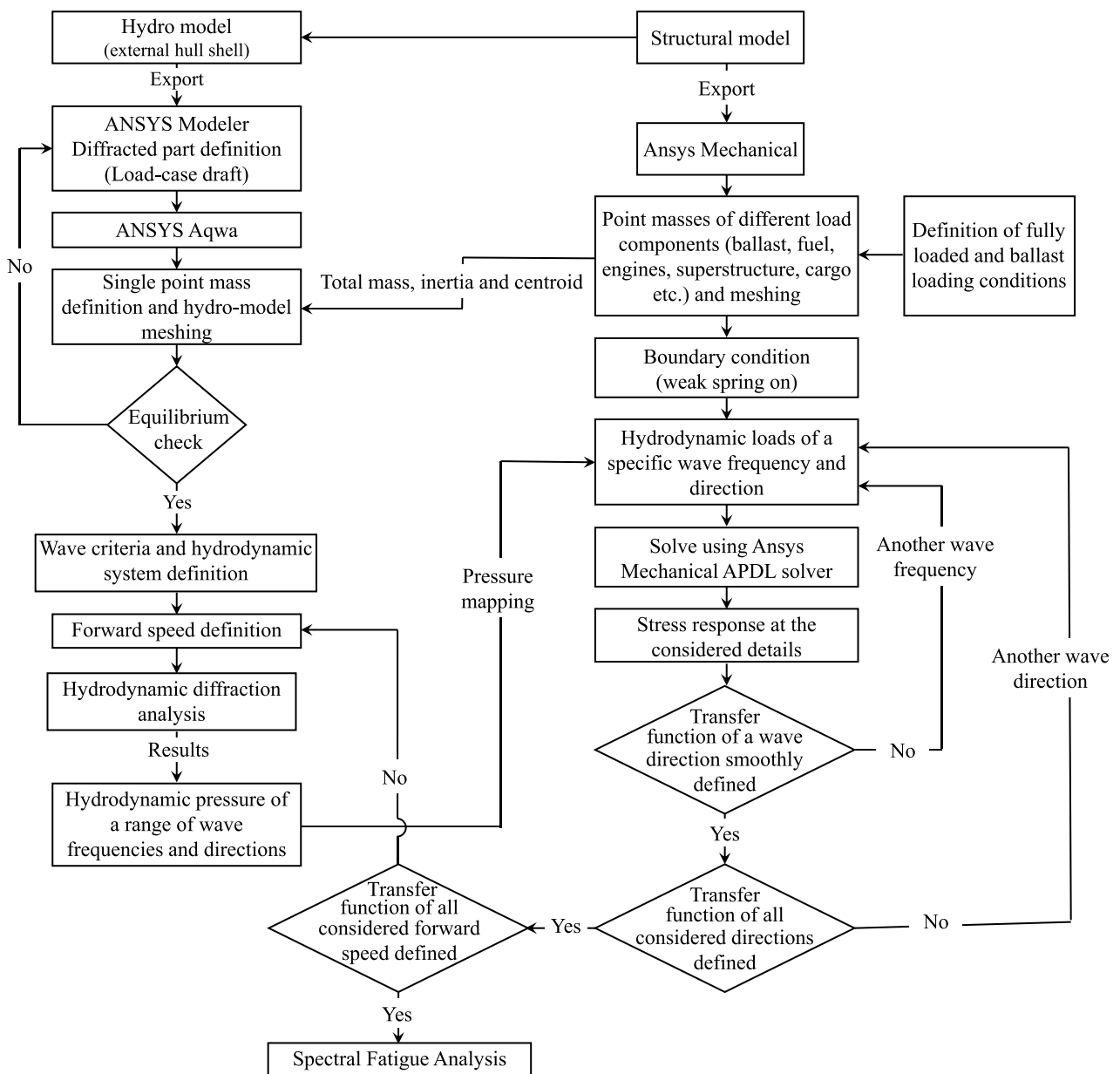


Fig. 6. Flowchart for transfer functions formation of one loading condition.

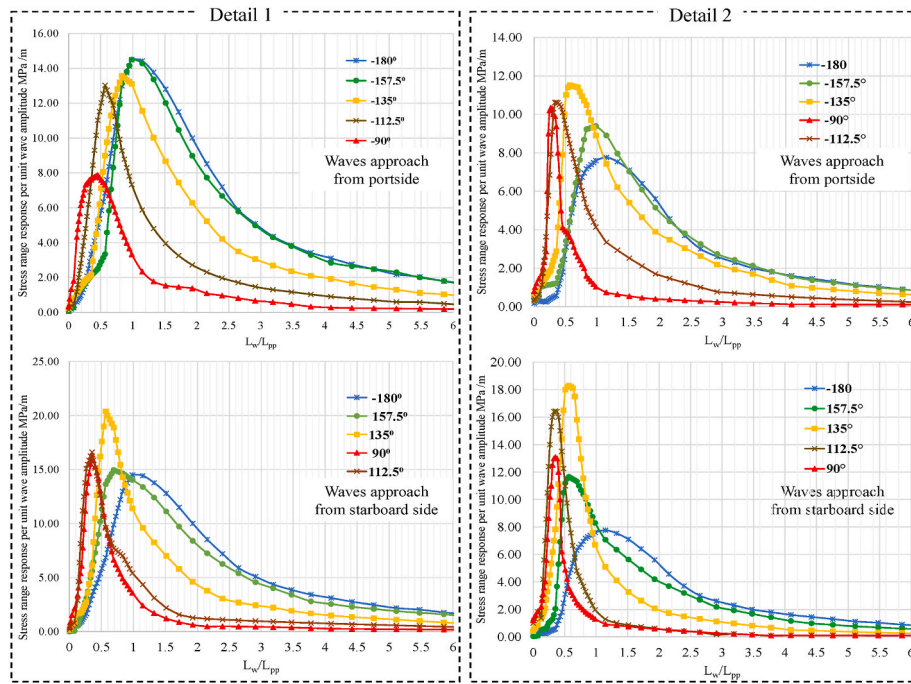


Fig. 7. Stress range per unit wave amplitude of detail 1 and 2, as a function of different wave heading directions and for zero forward speed and fully loaded condition.

obtained from the finite element analysis is the maximum normal stress in x-direction per unit wave amplitude at the considered details. Fig. 7 demonstrates the stress ranges at detail 1 and 2 for all wave directions of the fully-loaded condition at zero forward speed. It can be observed that the maximum stress response per unit wave amplitude is related to oblique and beam seas encountered from the same direction of the considered structural detail (starboard side). However, the maximum response of the beam seas occurs at high frequencies (small wavelength L_w/L_{pp}) close to the rolling resonance frequency of the ship which has low probability for high wave amplitudes. On the other hand, waves encountered from the opposite directions (Portside) show a systematic

reduction of the stress response peak and energy with the wave direction at detail 1. Fig. 8 illustrates the stress response corresponding to the hydrodynamic pressure in Fig. 4.

The effect of ship forward speed on the stress response of detail 1 is illustrated in Fig. 9 for head seas and fully loaded condition. It can be observed that the maximum stress range per unit wave amplitude increases with increasing the ship forward speed, while the peak value is shifted slightly towards lower wave frequencies (higher L_w/L_{pp}) with increasing the forward speed.

As the corrosion takes place on the internal and external surfaces of the structural elements, the hull girder section modulus HGSM decreases

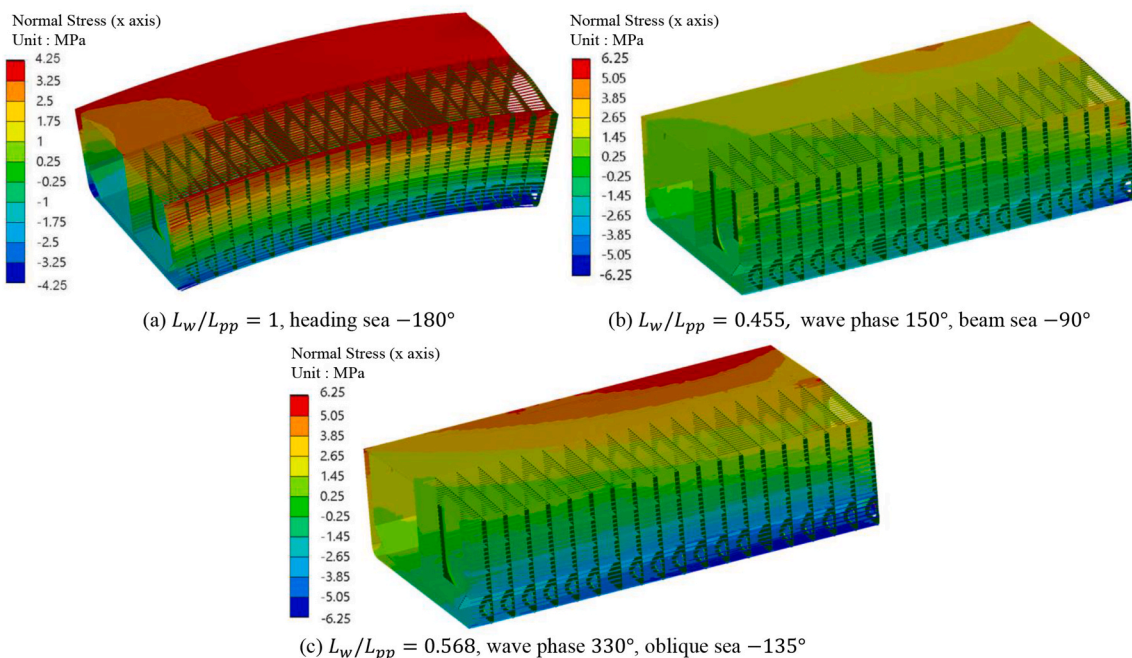


Fig. 8. Contours of normal stress response in x-direction corresponding to hydrodynamic pressure in Fig. 4.

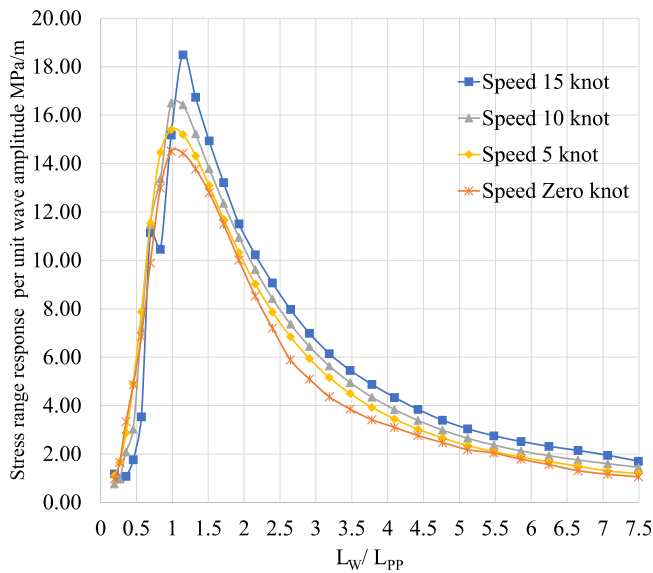


Fig. 9. Stress range per unit wave amplitude as a function of L_w / L_{pp} and forward speed for head seas (fully loaded condition, Detail 1).

over time and so does the hull girder strength. Uniform corrosion wastage was assumed for all the structural members of the considered hull module with corrosion rate as proposed by Wang et al. (Guo et al., 2008) model. Based on this assumption, the section modulus reduction $R_m(t)$ as a function of time t is obtained as:

$$R_m(t) = 0.62(t - 6.5)^{0.67} / 100 \quad (24)$$

This equation is obtained based on statistical analysis on corrosion wastage databases of single-hull oil tankers. It is noteworthy that, the beginning of the effective reduction of hull girder section modulus was assumed after 6.5 years of operation.

The hull girder section modulus loss throughout the ship's life is illustrated in Fig. 10 (a). This reduction will increase the nominal stress at the considered structural details presented in Fig. 2. The increment of the stress responses as a function of time is obtained by repeating the stress response analysis at different ages and fitting the results to an appropriate exponential function (Fig. 10 b and c). It is noteworthy that the observed stress increment in structural details below the design waterline, e.g., in bilge plate and bottom structure, was remarkably higher than that in details above the waterline. This can be explained by the fact that the corroded structures below the waterline is subjected to direct static and dynamic pressure; thus, the thickness reduction in this area should have a relatively higher impact.

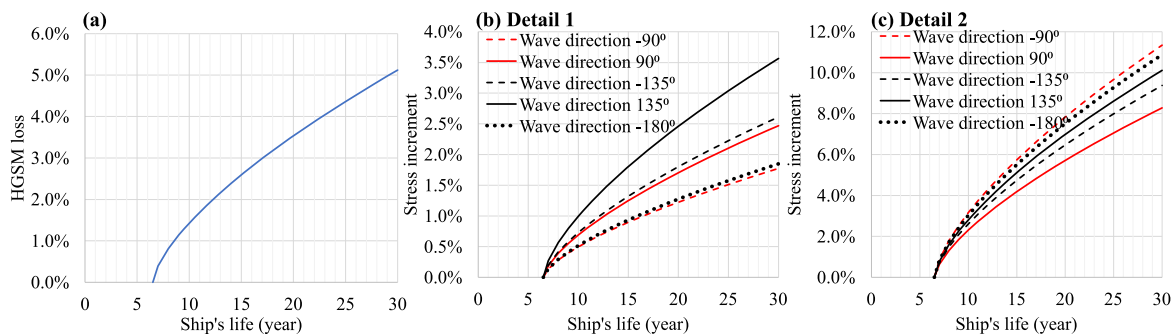


Fig. 10. (a) Hull girder section modulus loss due to an assumed uniform corrosion wastage (b and c) Stress increment due to corrosion as a function of ship's life for details 1 and 2, respectively (fully loaded condition).

4. Fatigue life of the considered details

The fatigue life depends on many parameters that may affect the fatigue damage significantly. The selected design wave scatter, corrosion fatigue and stress concentration are the main factors that have a considerable impact on the estimated accumulated fatigue damage. The high residual stresses of the welded joints may eliminate the need for mean stress correction, which in turn leads to shorter numerical fatigue life. The influences of those parameters on the fatigue damage of detail 1 are investigated for both the North Atlantic (NA) and the worldwide (WW) wave scatter diagrams, while the fatigue damage of detail 2 is only investigated for the Worldwide wave scatter diagram (WW) and Pierson–Moskowitz spectrum (P-M) without mean stress correction. A MATLAB code is created for the implementation of the above-described mathematical calculations.

Based on the performed analysis, the correlation between the accumulated fatigue damage through the ship's life and the considered wave scatter diagrams and wave spectra, with and without mean stress correction, is presented in Fig. 11. The figure also illustrates the impact of corrosion fatigue on the accumulated fatigue damage. It can be shown that the most severe accumulated fatigue damage is associated with the North Atlantic wave scatter diagram, while the worldwide wave scatter diagram usually shows lower accumulated damage. There is nearly 4–10 years difference in fatigue life considering each of these scatter diagrams. As may be seen from Fig. 11 (a), the maximum expected fatigue life is nearly 15.75 years for the world-wide wave scatter diagram together with P-M wave spectrum and mean stress correction. It is clear that the fatigue life decreases to nearly 11.75 years without mean stress correction, Fig. 11 (b). The application of the corrosion S–N curve after 6.5 years causes a higher accumulated fatigue damage rate (Fig. 11 a,b), which indicates the high sensitivity to the adopted corrosion S–N curve. The application of the corrosion S–N curve in the last 5 years of the ship's design life results in acceptable or relatively lower accumulated fatigue damage (Fig. 11 c,d). Therefore, it can be concluded that vessels exposed to weather conditions of various severity are advised to avoid extreme storm conditions (Sternsson and Bjökenstam, 2002) (weather routing) and regularly maintain the coating protection system, particularly, in ballast tanks in order to achieve a significant reduction in the probability of fatigue damage. Thus, in the following, results corresponding to the application of the corrosion S–N curve in the last 5 years are considered only.

The adopted environmental spectra in this study do not show a wide difference in the estimated fatigue life. The same observations were also reported by Nguyen et al. (2013). Nevertheless, the JONSWAP spectrum of fixed shape parameter is the most conservative spectrum, while its variable shape parameter form results in almost the same damage of P-M spectrum as a wide range of $T_p / \sqrt{H_s}$ is corresponding to $\gamma_J = 1$.

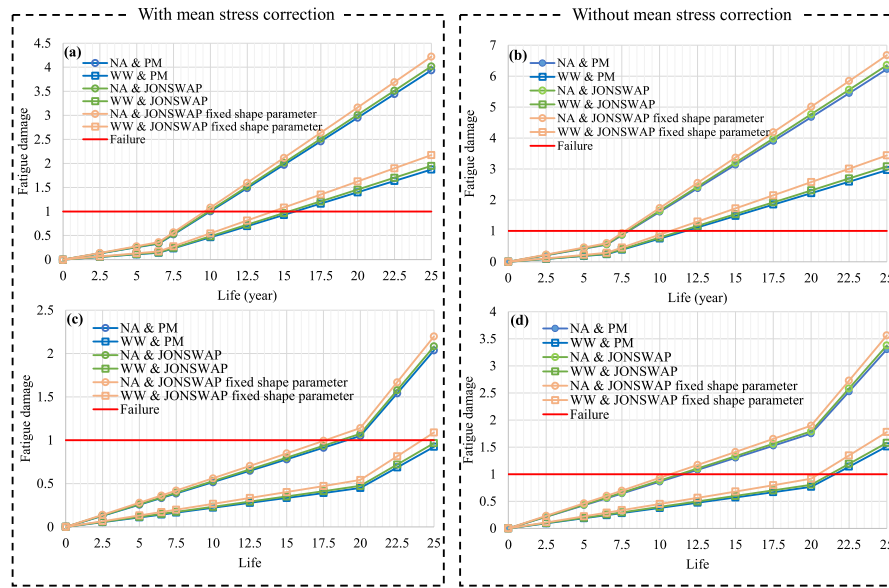


Fig. 11. Accumulated fatigue damage with and without mean stress correction for different wave scatter diagrams and wave spectra (fully loaded and ballast conditions); a and b, corrosion S–N curve is applied at the age of 6.5 years old; c and d, corrosion S–N curve is applied in the last 5 years of the design life (Detail 1).

4.1. Contribution of HGSM loss to the accumulated fatigue damage

After investigating the impact of corrosion fatigue on ship’s life, it is necessary to study the sensitivity of fatigue damage to the corrosion deterioration as a thickness reduction mechanism only. As discussed earlier in Fig. 10, the influence of corrosion as a uniform thickness reduction mechanism resulted in a slight and gradual increment in the stress response through the ship’s life. This increment initiates after the protective coating breakdown and reaches a maximum of 3% for detail 1 and 9.7% for detail 2 at the end of the ship’s life (25 years). This gradual increment of the stress response appears as a slight and negligible change in the slope of detail 1 damage curve (Fig. 12 a). However, detail 2 (Fig. 12 b), which is subject to external pressure from water and waves, experiences slightly higher damage due to the HGSM loss. This damage decreased the fatigue life by 1 year before the occurrence of the theoretical failure. For both details, the corrosion fatigue (or local corrosion at the hotspots of the structural details) shows a steeper damage curve after 20 years. Therefore, regular maintenance of the corrosion protection system is essential to eliminate the free corrosion and improve the fatigue life of the structural details in corrosive environments.

4.2. Wave heights contribution to fatigue damage

The contribution of the sea states with different significant wave heights H_s and periods T_z to the accumulated fatigue damage for each of the North Atlantic and Worldwide wave scatter diagrams is shown in Fig. 13. It can be observed that the wave heights from 3.5 m to 7.5 m

have the highest contribution to the total accumulated fatigue damage. The same observations were also reported in several studies (Magoga, 2020; Nguyen et al., 2013; Li et al., 2013).

4.3. Forward speed reduction

Carrying out the direct spectral fatigue analysis for several forward speeds requires solving the hydrodynamic diffraction and the finite element analyses as many times as the involved number of speeds. DNV (DNV CN, 2014) suggests applying only a single constant forward speed equals two-third of the service speed in the fully-loaded and ballast conditions. This speed may vary among the design standards. For instance, ABS (2009) suggests a speed of three-fourths of the service speed; while several studies performed the spectral fatigue analysis using zero forward speed. In this study, the fatigue damage considering zero-forward speed, 10 knot forward speed (2/3 of the design speed) and several forward speeds, as described in section 3.1, are compared in Fig. 14. The damage resulted from the adoption of 2/3 the ship design speed equals to that resulted from the reduction of ship speed based on the wave heights during the navigation. This is due to the high probability of the intermediate wave heights (when the forward speed is 2/3 of the design speed), while the high damage from severe sea states (zero forward speed) compensates the low damage from sea states of very small wave heights (design speed). On the other hand, applying zero forward speed gives slightly less conservative fatigue damage.

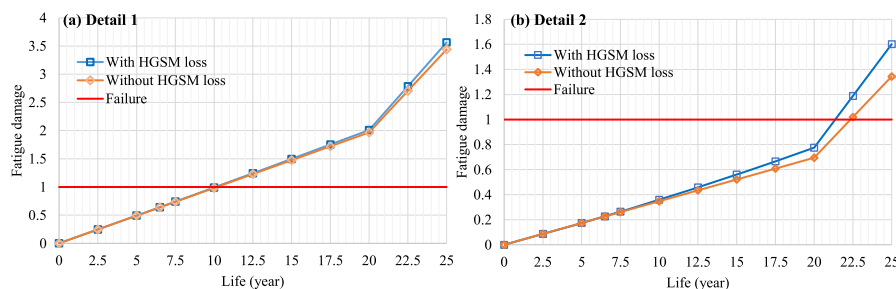


Fig. 12. Comparison between fatigue damage with and without hull girder section modulus loss.

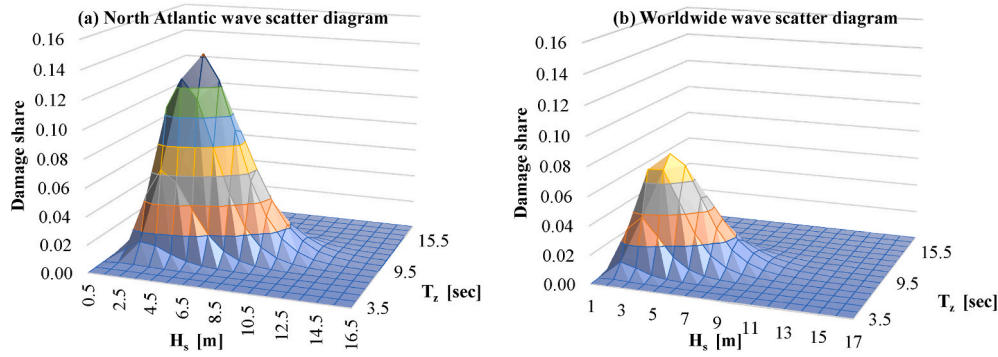


Fig. 13. Contribution of significant wave height H_s and wave period T_z to the total accumulated fatigue damage considering P-M wave spectra (a) North Atlantic, (b) Worldwide wave scatter diagram (Detail 1).

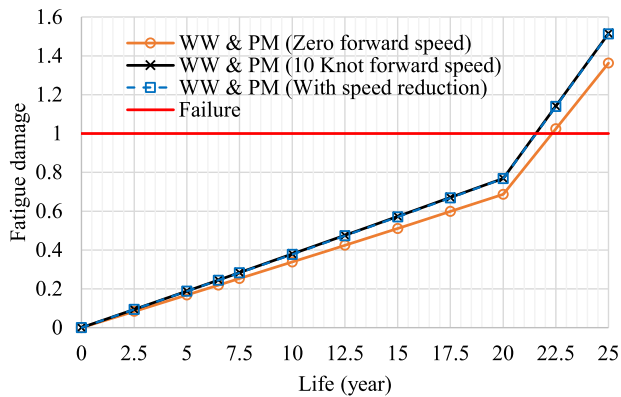


Fig. 14. Comparison between the SFA accumulated damage when applying a single forward speed (zero and 10 knots) and several speeds based on the sea state significant wave height (Detail 1).

4.4. Fatigue damage of detail 2

The fatigue damage of detail 2 is carried out considering a single forward speed only (2/3 of the design speed) and then it is compared with the corresponding fatigue damage of detail 1 as seen in Fig. 15. Although the fatigue damage of detail 1 is slightly smaller than that of detail 2, there is a huge contrast between the contributions of the fully loaded and the ballast conditions to the total fatigue damage of both details as explained in section 4.5.

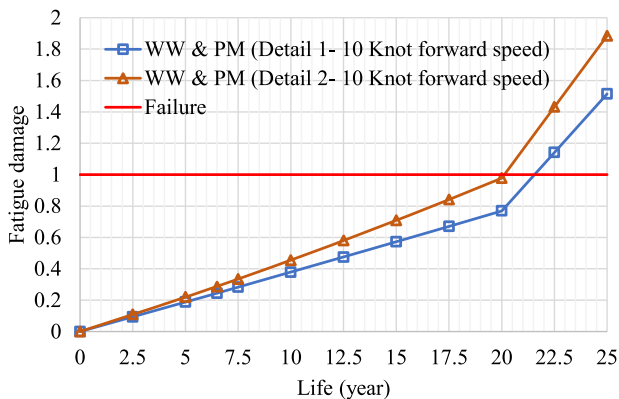


Fig. 15. Fatigue damage of detail 1 and detail 2 considering a single forward speed, 2/3 of the design speed.

4.5. Fatigue damage of the fully loaded and ballast conditions

Another important parameter that affects the accumulated fatigue damage is the loading condition. The contribution of the ballast and fully loaded conditions to the accumulated fatigue damage is illustrated in Fig. 16. The summation of the damages from the ballast and fully loaded conditions gives the total damage illustrated in Fig. 11. It can be observed that the ballast condition has a lower contribution to the fatigue damage of detail 1; and vice versa for detail 2. For instance, in detail 1, considering WW wave scatter diagram and P-M wave spectrum, the contribution of the fully loaded condition to fatigue damage is about twice the contribution of the ballast condition. On the other hand, the contribution of the ballast condition to fatigue damage of detail 2 is more than 2.5 times the contribution of the fully loaded condition. It has to be stressed that the high fatigue damage in ballast condition in detail 2 is mainly due to beam seas.

4.6. Single slope and Bi-linear S-N curve

Adopting a one slope S-N curve will result in little conservative results as illustrated in Fig. 17 for both North Atlantic and World-Wide wave scatter diagrams. The difference increases with increasing the probability of encountering waves of small heights which result in a stress range less than the endurance limit. Therefore, the fatigue damage obtained based on the North Atlantic wave scatter diagram is less sensitive to the type of the S-N curve as compared with that obtained based on the Worldwide scatter diagram.

4.7. Stress concentration factor

The estimated K_g is another important factor that has an exponential impact on the fatigue life as shown in Fig. 18. Therefore, decreasing the value of K_g can increase the fatigue life considerably which may be achieved during the design and construction stages (DNV CN, 2014).

5. Conclusion

The spectral fatigue analysis approach was adopted to investigate the accumulated fatigue damage of two structural details, below and above the mean waterline, in the side of a crude oil tanker. The calculated hydrodynamic pressure acting on the hull due to different wave directions and frequencies and forward speeds was mapped on the hull surface of the structural finite element model containing the main structural members. The stress response of the considered structural detail was derived for all the operational profiles and environmental conditions. The fatigue life was investigated for different wave scatter diagrams and wave spectrums.

It was demonstrated that the stress concentration factor and the mean stress correction have a considerable impact on the accumulated

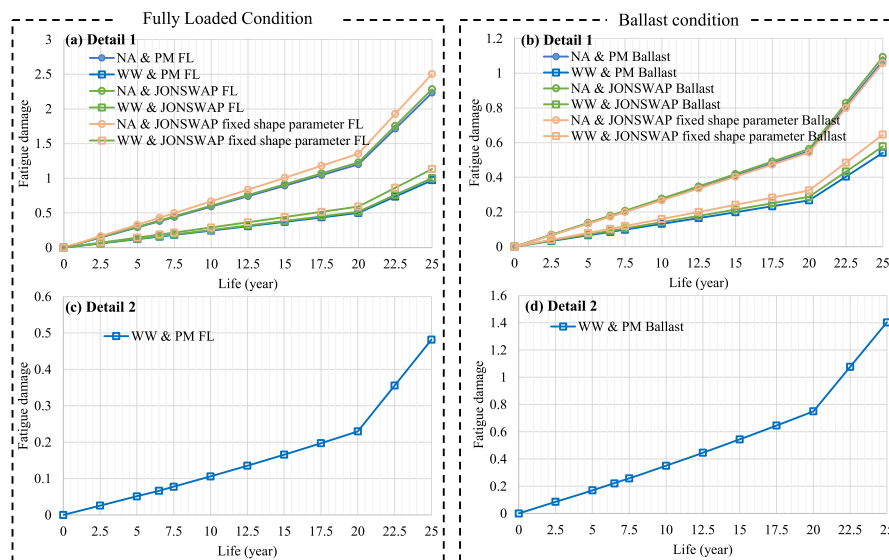


Fig. 16. Fatigue damage without mean stress correction for Fully Loaded (FL) and Ballast condition; corrosion S-N curve is applied in the last 5 years of the design life; a and b for detail 1; c and d for detail 2.

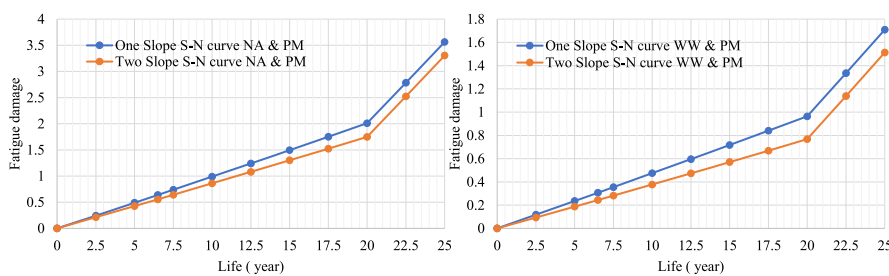


Fig. 17. Fatigue damage based on a single slope and a bi-linear S-N curves, employing NA and WW scatter diagrams and PM wave spectrum (detail 1).

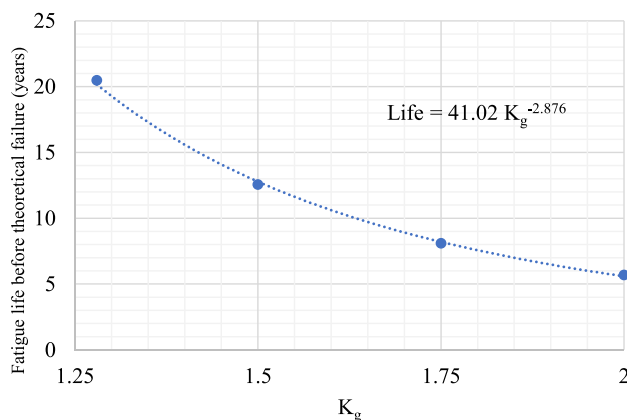


Fig. 18. Influence of K_g on the accumulated damage for Worldwide wave scatter diagram and P-M spectrum without mean stress correction (Detail 2).

fatigue damage. The spectral fatigue analysis taking into account the various ship speeds profile gives the same fatigue damage obtained by considering only a single forward speed equals 2/3 of the ship design speed.

The reduction of the hull girder section modulus due to uniform corrosion doesn't have a remarkable effect on fatigue life, particularly for structural details above the mean waterline. However, the free corrosion S-N curve has a significant effect and decreases the estimated

fatigue life considerably. The results depict that the estimated accumulated fatigue damage every 2.5 years using the free corrosion S-N curve is about three times that calculated using the S-N curve in air.

The paper demonstrated the main uncertainties in the spectral fatigue analysis, hence, accurate evaluation of these uncertainties can increase the reliability of the estimated accumulated damage. Further work should include time-domain fatigue analysis in locations near splash zones to study the uncertainties induced by the dynamic pressure due to the intermittent wet and dry surface. Finally, the spectral fatigue analysis needs intensive computations. However, using the finite element analysis, assessment of the fatigue damage of many structural details can be performed simultaneously within almost the same computational time needed for a single structural detail.

CRedit authorship contribution statement

A. Yosri: Methodology, Conceptualization, Visualization, Software, Formal analysis, Validation, Writing – original draft. **H. Leheta:** Methodology, Writing – review & editing, Supervision. **S. Saad-Eldeen:** Writing – review & editing, Validation, Supervision. **A. Zayed:** Writing – review & editing, Software, Validation, Supervision.

Declaration of competing interest

The authors declare that they have no known competing financial interests or personal relationships that could have appeared to influence the work reported in this paper.

References

- Aeran, A., Siriwardane, S.C., Mikkelsen, O., Langen, I., 2017. Life extension of ageing offshore structures: a framework for remaining life estimation. In: International Conference on Offshore Mechanics and Arctic Engineering. American Society of Mechanical Engineers, p. V03AT2A040.
- American Bureau of Shipping, 2003. Guide for the Fatigue Assessment of Offshore Structures. Houston.
- ANSYS Aqwa, 2013. AQWA Theory Manual, vol. 15317. Canonsburg, PA, USA.
- DNVGL, 2015. Class Guideline DNVGL-CG-0129: "Fatigue Assessment of Ship Structures". DNVGL, Oslo.
- DNVGL, 2018. Wave Loads. DNVGL-CG-0130 CLASS GUIDELINE, January.
- Bai, Y., Jin, W.-L., 2015. Marine Structural Design. Butterworth-Heinemann.
- Du, J., Li, H., Zhang, M., Wang, S., 2015. A novel hybrid frequency-time domain method for the fatigue damage assessment of offshore structures. *Ocean Eng.* 98, 57–65.
- Folsø, R., 1998. Spectral fatigue damage calculation in the side shells of ships, with due account taken of the effect of alternating wet and dry areas. *Mar. Struct.* 11, 319–343.
- Fricke, W., Wittenberg, L., 1995. An Integrated Approach for Fatigue Analysis of Tankers: the Second International Conference & Exhibition on Maritime Technology. ICMT '95), Singapore.
- Fricke, W., Scharrer, M., Von Selle, H., 1995. Integrated fatigue analysis of tanker structures. In: 6th International Symposium on Practical Design of Ships and Mobile Units, Seoul.
- Garbatov, Y., Guedes Soares, C., 2012. Uncertainty assessment of fatigue damage of welded ship structural joints. *Eng. Struct.* 322–333.
- Garbatov, Y., Guedes Soares, C., Parunov, J., Kodvanj, J., 2014a. Tensile strength assessment of corroded small scale specimens. *Corrosion Sci.* 85, 296–303.
- Garbatov, Y., Guedes Soares, C., Parunov, J., 2014b. Fatigue strength experiments of corroded small scale steel specimens. *Int. J. Fatig.* 59, 137–144.
- Garbatov, Y., Saad-Eldeen, S., Guedes Soares, C., Parunov, J., Kodvanj, J., 2019. Tensile test analysis of corroded cleaned aged steel specimens. *Corrosion Eng. Sci. Technol.* 54, 154–162.
- Guedes Soares, C., 1993. Long term distribution of non-linear wave induced vertical bending moments. *Mar. Struct.* 6, 475–483.
- Guedes Soares, C., 1995. Effect of wave directionality on long-term wave-induced loads effects in ships. *J. Ship Res.* 39, 150–159.
- Guedes Soares, C., Garbatov, Y., 1999. Reliability of maintained, corrosion protected plates subjected to non-linear corrosion and compressive loads. *Mar. Struct.* 12, 425–445.
- Guedes Soares, C., Schellin, T., 1998. Nonlinear Effects on Long-Term Distributions of Wave-Induced Loads for Tankers.
- Guedes Soares, C., Garbatov, Y., Von Selle, H., 2003. Fatigue damage assessment of ship structures based on the long-term distribution of local stresses. *Int. Shipbuild. Prog.* 50, 35–55.
- Guo, J., Wang, G., Ivanov, L., Perakis, A.N., 2008. Time-varying ultimate strength of aging tanker deck plate considering corrosion effect. *Mar. Struct.* 21, 402–419.
- Hasselmann, K., Barnett, T., Bouws, E., Carlson, H., Cartwright, D., Enke, K., et al., 1973. Measurements of wind-wave growth and swell decay during the Joint North Sea Wave Project (JONSWAP). *Ergänzungsheft* 8–12.
- Kukkanen, T., Mikkola, T.P., 2004. Fatigue assessment by spectral approach for the ISSC comparative study of the hatch cover bearing pad. *Mar. Struct.* 17, 75–90.
- DNV GL RP-C203, 2014. Fatigue Design of Offshore Steel Structures. RP-0005:2014-06.
- DNV, 2014. Classification Notes No. 30.7: Fatigue Assessment of Ship Structures. Det Norske Veritas Høvik, Norway, pp. 42–44.
- Li, S.-X., Akid, R., 2013. Corrosion fatigue life prediction of a steel shaft material in seawater. *Engineering Failure Analysis* 34, 324–334.
- Li, Z., Ringsberg, J.W., Storhaug, G., 2013. Time-domain fatigue assessment of ship side-shell structures. *Int. J. Fatig.* 55, 276–290.
- Lotsberg, I., 2019. Development of fatigue design standards for marine structures. *J. Offshore Mech. Arctic Eng.* 141.
- Magoga, T., 2020. Fatigue damage sensitivity analysis of a naval high speed light craft via spectral fatigue analysis. *Ships Offshore Struct.* 15, 236–248.
- Nguyen, K.T., Garbatov, Y., Guedes Soares, C., 2012. Fatigue damage assessment of corroded oil tanker details based on global and local stress approaches. *Int. J. Fatig.* 43, 197–206.
- Nguyen, K.T., Garbatov, Y., Soares, C.G., 2013. Spectral fatigue damage assessment of tanker deck structural detail subjected to time-dependent corrosion. *Int. J. Fatig.* 48, 147–155.
- ABS, October 2017. Spectral-based Fatigue Analysis for Vessels. American Bureau of Shipping.
- Rörup, J., 2005. Mean compressive stresses - experimental and theoretical investigations into their influence on the fatigue strength of welded structures. *J. Strain Anal. Eng. Des.* 40, 631–642.
- Rörup, J., Garbatov, Y., Dong, Y., Uzunoglu, E., Parmentier, G., Andoniu, A., et al., 2017. Round Robin Study on Spectral Fatigue Assessment of Butt-Welded Joints, pp. 663–671.
- Santecchia, E., Hamouda, A.M.S., Musharavati, F., Zalnezhad, E., Cabibbo, M., El Mehtedi, M., et al., 2016. A review on fatigue life prediction methods for metals. *Adv. Mater. Sci. Eng.* 2016, 9573524.
- Sarkani, S., Kihl, D., Beach, J., 1994. Fatigue of welded joints under narrowband non-Gaussian loadings. *Probabilist. Eng. Mech.* 9, 179–190.
- Shetty, N.K., 1997. Probabilistic Fatigue Assessment of Welded Joints. *Probabilistic Methods for Structural Design*. Springer, pp. 85–111.
- Sternsson, M., Bjökenstam, U., 2002. Influence of weather routing on encountered wave heights. *Int. Shipbuild. Prog.* 49, 85–94.
- Thompson, I., 2016. Validation of naval vessel spectral fatigue analysis using full-scale measurements. *Mar. Struct.* 49, 256–268.
- ABS, 2009. Guidance Notes on Spectral-Based Fatigue Analysis for Vessels, vol. 2004. American Bureau of Shipping. Updated.
- Wang, Y., 2010. Spectral fatigue analysis of a ship structural detail—A practical case study. *Int. J. Fatig.* 32, 310–317.
- Webster, G., Ezeilo, A., 2001. Residual stress distributions and their influence on fatigue lifetimes. *Int. J. Fatig.* 23, 375–383.
- Wirsching, P.H., Chen, Y.-N., 1988. Considerations of probability-based fatigue design for marine structures. *Mar. Struct.* 1, 23–45.
- Xue, J., Pittaluga, A., Cervetto, D., 1994. Fatigue damage calculation for oil tanker and container ship structures. *Mar. Struct.* 7, 499–535.
- Yosri, A., Zayed, A., Saad-Eldeen, S., Leheta, H., 2020. FATIGUE ASSESSMENT OF AGED STEEL SPECIMENS UNDER UNIAXIAL CYCLIC LOADING. Springer, pp. 523–532.
- Yosri, A., Zayed, A., Saad-Eldeen, S., Leheta, H., 2021. Influence of stress concentration on fatigue life of corroded specimens under uniaxial cyclic loading. *Alex. Eng. J.* 60, 5205–5216.
- Yue, J., Yang, K., Peng, L., Guo, Y., 2021. A frequency-time domain method for ship fatigue damage assessment. *Ocean Eng.* 220, 108154.